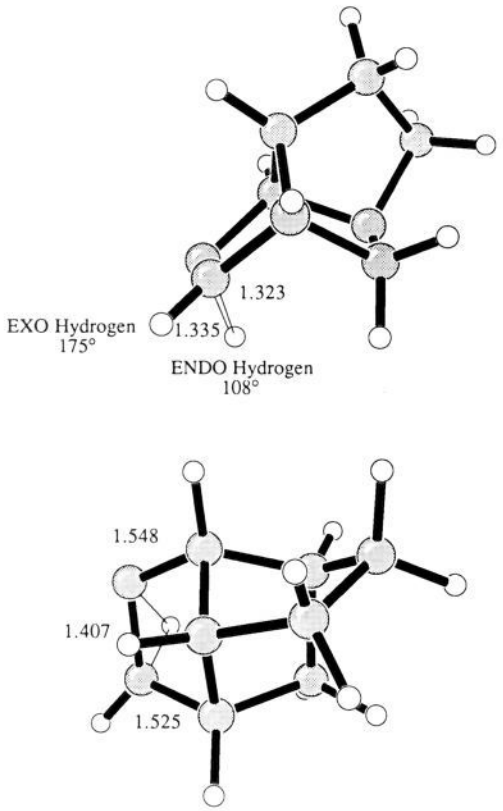

Figure 16. Brexan-5-ylidene endo transition structure (RHF/3-21G).

this interaction, as compared to the 0.4 kcal/mol computed for carbena-2-norbornane. The closest nonbonded hydrogen interaction distance involving the migrating endo hydrogen is 2.30 Å for the brexan-5-ylidene endo transition structure and 2.58 Å for carbena-2-norbornane. The MM2 van der Waals energies are 0.7 and 0.1 kcal/mol, respectively. There is 0.4 kcal/mol less nonbonded replusion in the exo transition structure of brexan-5-ylidene than in the endo transition structure. This exo preference is 0.7 kcal/mol larger than in carbena-2-norbornane.

Conclusion

Ground-state alignment has little influence on the rates of hydrogen 1,2-shifts in carbenes. The significant eclipsing of the partial bonds that develops in the endo transition structures is thought to be the origin of exo selectivity in the norbornane structures. The twist induced by the additional ethane bridge in brexan-5-ylidene modifies the alignment of the exo and endo hydrogens, along with the nonbonded interaction sites that are found to determine the unusually high selectivity of this system. Theoretical calculations predict the exo (axial) and endo (equatorial) activation barriers of larger carbene systems: dimethylcarbene (6.0 kcal/mol), cyclohexylidene (−0.1 and 0.0 kcal/mol), carbena-2-norbornane (7.2 and 9.0 kcal/mol), carbena-2-norbornene (9.2 and 11.3 kcal/mol), and brexan-5-ylidene (6.3 and 9.1 kcal/mol). Because tunneling will enhance rates of hydrogen shifts in carbenes, measured barriers may prove to be even lower than these.[21]

Acknowledgment. We are grateful to the National Science Foundation for financial support of this research and to Professor Alex Nickon of Johns Hopkins University for helpful discussions. This work was supported in part by a grant of computer time made possible under a joint study with the IBM Corp. on the IBM 3090/600J Supercomputer at the UCLA Office of Academic Computing. Dr. Michael Miller provided the graphics for Figures 2-16.

(21) Osamura, Y.; Schaefer, H. F., III; Gray, S. K.; Miller, W. H. *J. Am. Chem. Soc.* **1981**, *103*, 1904. Gray, S. K.; Miller, W. H.; Yamaguchi, Y.; Schaefer, H. F., III. *Ibid.* **1981**, *103*, 1900.

Electron Affinity of O^- and Diabatic CaO(g) Integer Charge Potential Curves

David P. Baldwin,*,† Ernest J. Hill, and Robert W. Field

Contribution from the George R. Harrison Spectroscopy Laboratory and the Department of Chemistry, Massachusetts Institute of Technology, Cambridge, Massachusetts 02139.
Received April 13, 1990

Abstract: A ligand field, integer-charge ionic model for the electronic structure of diatomic CaO(g) provides a basis for an empirical deperturbation of the lowest lying $^1\Sigma^+$ electronic states to their diabatic doubly charged ($Ca^{2+}O^{2-}$) and singly charged ionic (Ca^+O^-) potentials. The deperturbed doubly charged and lowest singly charged potentials cross at r_{Ca-O} = 2.16 (1) Å at an energy 10 400 (100) cm^{-1} above v = 0 of the experimentally observed $X^1\Sigma^+$ ground state. The interaction matrix elements between the three lowest interacting $^1\Sigma^+$ states have been determined as functions of r_{Ca-O}. With use of a simple Rittner model for the diabatic curves, extrapolation to infinite internuclear separation yields a value for the electron affinity of O^- (i.e., $O^- + e^- \rightarrow O^{2-}$) of −4.53 (6) eV, in agreement with quantum-chemical results, and a value of 35 160 (200) cm^{-1} for D_0^0 of CaO, in excellent agreement with thermochemical values.

I. Introduction

The electronic spectra of the fourth-row, gas-phase, diatomic metal oxides are among the most complicated and congested diatomic spectra observed. Assignment of transitions and derivation of molecular constants from these spectra, which often contain rovibronic transitions with a spectral density of >10 lines/cm^{-1} over the entire visible region, has largely become possible only with the advent of high resolution, tunable, visible wavelength lasers and multiple resonance and selectively detected excitation techniques. Even with the present ability to derive molecular constants from strongly perturbed and dense spectra, with few exceptions it has not been possible to go beyond the molecular constants of individual electronic states to a global

† Current address: Combustion Research Facility, Sandia National Laboratories, Livermore, CA.

0002-7863/90/1512-9156$02.50/0

Table I. Molecular Constants[a] for the $^1\Sigma^+$ States of CaO

state[c]	T_0	B_e	α_e	ω_e	$\omega_e x_e$	ref
$X^1\Sigma^+$	0	0.4445	0.0034	733.4	5.28	7, 25
X*	450 (100)	0.464 (1)	0.0003	732 (6)	0.66 (3)	*b*
$A^1\Sigma^+$	11549	0.4059	0.0014	718.9	2.11	7, 25
A*	9526 (100)	0.3727	0.0028	579.8	3.2	2, 3, 4, 6, 8
$C'^1\Sigma^+$	24636	0.3455	0.0024	550.4	2.84	5
$C^1\Sigma^+$	28772	0.3731	0.0032	560.9	4.0	10
C*	28368 (100)	0.3858	0.0043	539.5	3.74	11, 26, 27

[a] All constants are given in cm^{-1}. [b] Constants for the X* state were determined by a least-squares fit to a Morse potential expression. These constants were NOT used in the determination of D_0^0(CaO) and EA(O^-). [c] States with asterisks are calculated (deperturbed) diabatic curves based on single-configuration ligand field model structures.

understanding of electronic structure. The ab initio and traditional spectroscopic models, which have been applied with considerable success to second- and third-row diatomics, give little insight into the structure of these systems and seldom provide predictions useful for interpreting unassigned spectra.

We base our zero-order picture of electronic structure in these systems on two simplifying steps. First, we adopt a ligand field or crystal field model, similar to those universally used for spectra of condensed phase systems. We view the metal oxides as integer-charge ionic (M^+O^- or $M^{2+}O^{2-}$) structures, and their electronic transitions as between metal-ion-centered atomic-ion orbitals. These orbitals are split, mixed, and shifted from their free-ion energies by an external charge localized on the O ligand center. Second, we apply this model to CaO, perhaps the simplest diatomic metal oxide that is expected to have both singly charged ionic (SCI) and doubly charged ionic (DCI) electronic states at low energies. The only low-lying, predominantly DCI electronic state of CaO is the $X^1\Sigma^+$ ground state. The remaining low-lying states (13 of 16 predicted states below 29000 cm^{-1} have been observed and analyzed) are all well described by an SCI structure with a single electron localized outside a closed shell Ca^{2+} core and a single p^{-1} hole localized on O^-. The electronic properties (i.e. orbital energies, spin–orbit couplings, and effective orbital angular momenta) of these isolated electron and hole structures may be (and have been) derived empirically from two SCI model molecules, CaF and NaO. These two are chosen since their valence states have similar internuclear distances, and therefore similar ligand field strengths, to those of the corresponding states of CaO.

The effects of a closed shell point-charge/induced dipole (F^-) on the Ca^+ structure have been discussed at length,[1] as has a similar treatment of O^- in the field of a compact, closed shell Na^+ atomic ion.[2] In the case of CaF, the F^- has the effect of splitting, shifting, and mixing low-lying Ca^+ 4s, 4p, and 3d atomic ion states, and in NaO, the closed shell Na^+ atomic ion lifts the degeneracy of the O^- p^{-1} hole π^{-1} and σ^{-1} orientations which retain their relatively pure oxygen 2p character. In our model, the molecular electronic configurations of CaO combine Ca^+ orbitals (named $X\sigma$, $A\pi$, and $B\sigma$ because their electronic properties are identical with those determined spectroscopically for the corresponding CaF $X^2\Sigma^+$, $A^2\Pi$, and $B^2\Sigma^+$ states) with O^- $p\pi^{-1}$ and $p\sigma^{-1}$ orbitals (the properties of which are derived from the $X^2\Pi$ and $A^2\Sigma^+$ states of NaO). For example, the $X\sigma\pi^{-1}$ configuration of CaO gives rise to the $a^3\Pi$ and $A'^1\Pi$ electronic states. This model predicts fine structure and interaction parameters in the spectrum of CaO in remarkable agreement with experimentally determined parameters.[3-6]

A further consequence of the separated single-electron/single-hole structure of CaO is the near degeneracy of all electronic states arising from each molecular configuration. This near degeneracy is a consequence of near-zero values of direct and exchange Coulomb integrals (inversely proportional to the electron/hole separation), which are very small for orbitals localized on different atomic centers because of the vanishingly small overlap between these orbitals. The vibrational and rotational constants for all electronic states within each configuration are also nearly identical. It is from these molecular constants that we construct Rydberg–Klein–Rees (RKR) potential curves to describe the interatomic potential energy as a function of internuclear separation. The expected and observed small splittings and similar potential energy curves for isoconfigurational states are the key to our zero-order integer-charge deperturbation model. We use observed potentials for states which by symmetry (i.e., not $^1\Sigma^+$) are free of SCI~DCI perturbation, as a basis for calculating deperturbed potentials for the isoconfigurational $^1\Sigma^+$ states strongly affected by the SCI~DCI interaction. When the molecular constants for an unperturbed state of a given configuration are not available, the ligand field model allows us to construct reference zero-order potentials from the constants of states belonging to other configurations based on the characteristic energy shifts and changes in molecular constants of the model SCI structures, CaF and NaO.

In this paper, we will use the deperturbation procedure outlined above to derive integer-charge diabatic potentials for the interacting predominantly DCI $X^1\Sigma^+$ ground state and the predominantly SCI $A^1\Sigma^+$ ($X\sigma\sigma^{-1}$), $C'^1\Sigma^+$ ($A\pi\pi^{-1}$), and $C^1\Sigma^+$ ($B\sigma\sigma^{-1}$) excited states. The only molecular electronic symmetry that may arise from the ground state of the Ca^{2+} and O^{2-} closed shell DCI atomic ions is $^1\Sigma^+$. Since only SCI and DCI states of identical symmetry can interact, *all of the low-lying states of symmetries other than $^1\Sigma^+$ are purely SCI and need not be deperturbed.* These non-$^1\Sigma^+$ potentials serve to define deperturbed reference potentials for the nominally SCI $^1\Sigma^+$ states. The deperturbed $^1\Sigma^+$ potentials, to be derived below, will give values for r_c(A~X), the internuclear distance at which the DCI and lowest SCI diabatic potentials cross; the potential energy at this crossing distance relative to the experimentally observed $X^1\Sigma^+$ ground state; and the diabatic electronic interaction matrix elements between the DCI and lowest SCI $^1\Sigma^+$ states, determined as functions of r. Because the diabatic potentials have experimentally well-defined energies relative to each other and to the minimum of the (perturbed) $X^1\Sigma^+$ potential, we will be able to use these potentials, extrapolated to infinite internuclear separation, to obtain values for both D_0^0 of CaO and the electron affinity of O^-. This extrapolation requires the inclusion of the effect of a third $^1\Sigma^+$ electronic state at large internuclear distance. These values will be found to be in good agreement with previous experimental and theoretical results.

II. Analysis; Calculation of Deperturbed Potentials

The $X\sigma\sigma^{-1}$ configuration gives rise to the lowest energy ($T_0(A^1\Sigma^+)$ = 11550 cm^{-1}) SCI $^1\Sigma^+$ state as well as the $b^3\Sigma^+$ electronic state. The RKR curve for the observed perturbed (i.e., mixed SCI–DCI) $A^1\Sigma^+$ state may be constructed from rotation-vibration constants (ω_e, $\omega_e x_e$, B_e, and α_e) previously reported by Hultin and Lagerqvist[7] (see Table I). Because of experimental difficulties in observing σ^{-1} triplet states, little was known about

(1) Rice, S. F.; Martin, H.; Field, R. W. *J. Chem. Phys.* **1985**, *82*, 5023–5034.
(2) Allison, J. N.; Cave, R. J.; Goddard, W. A., III *J. Phys. Chem.* **1984**, *88*, 1262–1268.
(3) Marks, R. F.; Gottscho, R. A.; Field, R. W. *Phys. Scr.* **1982**, *25*, 312–328.
(4) Norman, J. B.; Cross, K. J.; Schweda, H. S.; Polak, M.; Field, R. W. *Mol. Phys.* **1989**, *66*, 235–268.
(5) Baldwin, D. P.; Field, R. W. *J. Mol. Spectrosc.* **1989**, *133*, 90–95.
(6) Baldwin, D. P.; Norman, J. B.; Soltz, R. A.; Sur, A.; Field, R. W. *J. Mol. Spectrosc.* **1990**, *139*, 39–67.
(7) Hultin, M.; Lagerqvist, A. *Ark. Fys.* **1951**, *2*, 471–507.

the $b^3\Sigma^+$ electronic state of CaO until recently. A dispersed fluorescence study[8] has located $v = 1$ of this state and has given an energy ($T_1 = 10073$ cm^{-1}). To obtain vibrational and rotational constants for the $b^3\Sigma^+$ state, we use the values for the $a^3\Pi$ ($X\sigma\pi^{-1}$) state,[6] scaled by the ratios of σ^{-1} and π^{-1} state constants in NaO.[2] This scaling of the $a^3\Pi$ rotation–vibration constants gives the rotation and vibration constants shown in Table I for the deperturbed (i.e., purely SCI) $A^{*1}\Sigma^+$ state. The $b^3\Sigma^+$ potential curve constructed from these constants, shifted up in energy by a predicted $A^{*1}\Sigma^+ - b^3\Sigma^+$ exchange splitting[9] of 60 cm^{-1} and anchored to the single known vibrational level of the $b^3\Sigma^+$ state, gives the deperturbed diabatic curve, A*.

The second SCI $^1\Sigma^+$ state, $C'^1\Sigma^+$, arises from the $A\pi\pi^{-1}$ configuration. This state has been observed and fully analyzed,[5] and so have the five other electronic states ($^3\Sigma^+$, $^{1,3}\Sigma^-$, $^{1,3}\Delta$) that come from this configuration.[3,4,6] Unlike the $A^1\Sigma^+$ state, which lies ~2000 cm^{-1} above its isoconfigurational $^3\Sigma^+$ state, the $C'^1\Sigma^+$ state falls in the middle of the narrow range of energies ($\Delta T_0 = 567$ cm^{-1}) of this configuration, and its molecular constants also lie well within the range of constants for this configuration. We can therefore conclude, since we detect no significant deviation from the range of experimentally determined potentials for this configuration, that the $C'^1\Sigma^+$ state is not strongly perturbed by other $^1\Sigma^+$ states and in particular not by the $X^1\Sigma^+$ DCI state. We therefore ignore any contribution from the $C'^1\Sigma^+$ state to this perturbation.

The third SCI $^1\Sigma^+$ state, $C^1\Sigma^+$, arises from the $B\sigma\sigma^{-1}$ configuration. This state has been observed and analyzed[10] (see Table I). However, due to experimental difficulties in observing σ^{-1} triplet states, the isoconfigurational $B\sigma\sigma^{-1}$ $^3\Sigma^+$ reference state has not been observed or analyzed. It is therefore necessary to construct a deperturbed potential for this $^1\Sigma^+$ state based on the *atomic-ion-in-molecule* model. The rotational and vibrational constants used to construct this deperturbed C* potential are those of the $B^1\Pi$ ($A\pi\sigma^{-1}$) state of CaO, scaled for the $B\sigma\sigma^{-1}$ configuration by the ratios of CaF $B^2\Sigma^+$ and $A^2\Pi$ state molecular constants. The C* potential curve is thus placed above the derived A* ($X\sigma\sigma^{-1}$) potential at an energy equal to the CaF $B^2\Sigma^+ - X^2\Sigma^+$ energy interval. This gives the molecular constants in Table I for the deperturbed C* diabatic potential.

The $X^1\Sigma^+$ ground state has been extensively studied,[7,10] and its molecular constants are also reported in Table I. With use of the parameters in Table I, the RKR potentials for $v = 0$–15 for the X, A*, A, C*, and C states were calculated,[11] giving 300 energies at 300 different internuclear distances for each set of molecular constants (inner and outer turning points calculated for every 0.1 increment from $v = 0$–15). Deperturbation of the $X^1\Sigma^+$ state to the diabatic DCI potential X* was done graphically. Since the $X^1\Sigma^+$ state interacts significantly with only the $A^1\Sigma^+$ and $C^1\Sigma^+$ states, the X* DCI diabatic potential was obtained by adding the differences between the $A^1\Sigma^+$ and A* and $C^1\Sigma^+$ and C* potentials to the RKR $X^1\Sigma^+$ curve. Each of the calculated RKR potentials was fit to a quartic polynomial. These curves are shown in Figure 1, plotted over the range of internuclear distances from 1.61 to 2.35 Å. This range corresponds to the largest $v = 15$ inner turning point of the group of RKR curves and the smallest $v = 15$ outer turning point. The curves thus obtained show a crossing of the A* SCI diabatic and X* DCI diabatic potentials at 2.16 (1) Å at an energy $T_c(0) = 10400$ (100) cm^{-1} above $v = 0$ of the observed $X^1\Sigma^+$ state. Since the $C^1\Sigma^+$ curve does not deviate significantly from the C* curve at the internuclear distance where the A~X crossing occurs, the A~X crossing can be viewed as a two-state interaction. The interaction matrix element $H_{A\sim X}$ ($r = 2.16$ Å) determined with the use of perturbation theory is 5000 (100) cm^{-1}. $H_{A\sim X}$ and $H_{C\sim X}$ will be determined as functions of r_{Ca-O} in the next section, after a discussion of the exact nature of these diabatic curves and the matrix elements that couple them.

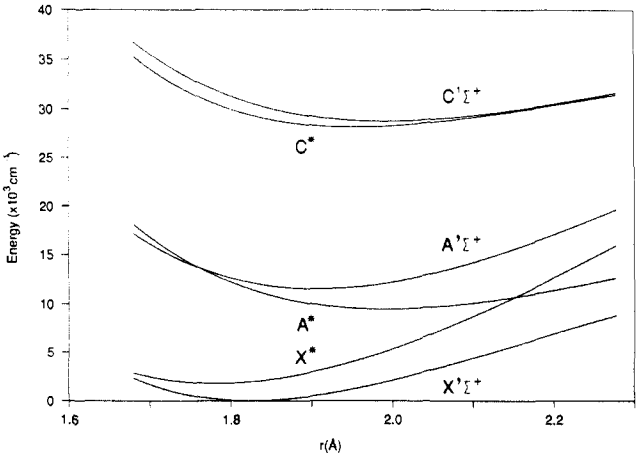

Figure 1. RKR potentials for the observed C, A, and $X^1\Sigma^+$ electronic states of CaO. The C* and A* potentials are singly-charged ionic, diabatic, deperturbed potentials for the C and A states based on the isolated atomic-ion model. The X* curve is the doubly-charged ionic, diabatic, deperturbed potential derived from the $X^1\Sigma^+$ potential by adding the A–A* and C–C* energy shifts.

III. Discussion

Diabatic Potentials. It is not possible to give a unique definition of a diabatic potential curve without identifying the specific terms in H_{el} that are to be excluded. The difficulties inherent in this process and the consequent nonuniqueness of the a priori definition of diabatic curves have been discussed in the literature.[30,31] Diabatic curves may, however, be defined empirically, and approximate descriptions of the implicitly excluded terms may be given, as will be done here.

The diabatic potential curves obtained in the previous section are based upon the localized atomic-ion orbitals of our *atomic-ion-in-molecule* model. The ab initio diabatic potentials of ref 9 are based on SCF single-configuration basis states where molecular orbitals are formed by allowing mixing of the Ca-centered and O-centered atomic orbitals. It is in this change of basis set that our model differs from this ab initio calculation. The single-configuration states from this calculation which have a minimum amount of Ca-orbital–O-orbital delocalization show the best agreement with the experimentally obtained results. The ab initio calculation of the $X^1\Sigma^+$ state with use of a single configuration showed the most Ca-orbital–O-orbital mixing and incorrectly predicted the energy ordering for this state. The ionic model employed here is a deperturbation of empirical potential curves which implicitly assumes a fundamentally different set of basis orbitals and therefore gives fundamentally different diabatic potentials.

The diabatic representation used here is the most convenient representation based upon our semiempirical model and the goal of deriving ionic interaction parameters and ionic properties (e.g., the electron affinity of O^-). The nature of this derivation defines this representation as diagonal in all parts of the electronic Hamiltonian, H_{el}, except the electron–electron and electron–nuclear DCI~SCI terms discussed in the following section. In particular, it should be noted that there are *by definition* no matrix elements of H_{el} between the A* and C* potentials.

Interaction Matrix Element. In our model, the interaction between the SCI and DCI configurations, in this case the $X\sigma\sigma^{-1}$ ($\sigma\sigma'$) and closed shell (σ^2) configurations, arises from electron–electron and electron–nuclear electrostatic matrix elements of the total electronic Hamiltonian. Electrostatic integrals of this type are often calculated for interactions of a Rydberg-type orbital with ion-core orbitals[12] or between atom-like orbitals centered on the

(8) Baldwin, D. P.; Field, R. W. *J. Mol. Spectrosc.* **1990**, *139*, 77–83.
(9) Bauschlicher, C. W., Jr.; Yarkony, D. R. *J. Chem. Phys.* **1978**, *68*, 3990–3997. Diffenderfer, R. N.; Yarkony, D. R. *J. Chem. Phys.* **1982**, *77*, 5573–5580.
(10) Lagerqvist, A. *Ark. Fys.* **1954**, *8*, 83–95.
(11) The RKR computer program was written by R. N. Zare and J. Cashion, UCRL Rept. No. UCRL-10881 (1963).
(12) Lefebvre-Brion, H.; Field, R. W. *Perturbations in the Spectra of Diatomic Molecules*; Academic Press: Orlando FL, 1986.

same nucleus, with some degree of accuracy. However, in the present problem, the integral is a two-center interaction between atomic-ion orbitals localized on well separated centers. Such a calculation would require a computation more sophisticated than the simplicity of our model warrants.

In the present case, we can view the interaction as arising from a phenomenological operator of the form

$$\langle \hat{H}_{el} \rangle = \langle \sigma' \sigma | 2e^2/r_{Ca-O} | \sigma^2 \rangle \quad (1)$$

where the primed orbital is centered on Ca and unprimed orbitals are centered on O. Here $r_{Ca-O}/2$ replaces the more exact r_{ij} because the interacting electrons (or interacting electron and nucleus) are localized on well-separated centers. $r_{Ca-O}/2$ is (crudely) the distance between the $\sigma\sigma'$ overlap region and the average position of the electron (or nucleus) of the O^- ligand. Note that this operator can introduce perturbations between SCI and DCI states precisely because *it is non-zero only if the real molecule deviates from the idealized model*; it depends on the existence of a non-zero overlap $\sigma'(1)\sigma(1)$ between a Ca- and an O-centered orbital. The other electrostatic terms in H_{el} (i.e., V_{NN} and the diagonal parts of V_{ee} and V_{eN}) do not depend on this overlap and thus are subsumed into the zero-order ligand-field Hamiltonian.

We can now understand the form of this matrix element and the approximate form of its variation with internuclear separation. From second-order perturbation theory, assuming a Coulomb electrostatic attractive form of the potential curves at $r \gg r_c(A \sim X)$, we obtain an expression for the second-order shift in energy of the adiabatic potentials from the derived diabatic curves proportional to r_{Ca-O}^{-1}:

$$\Delta E^{(2)} \approx \frac{|\langle \sigma'(1)\sigma(1)|e^2/r_{ij}|\sigma(2)\sigma(2)\rangle|^2}{4e^2/r_{Ca-O} - e^2/r_{Ca-O}} \approx \frac{|e^2 S_{\sigma\sigma'}(r_{Ca-O})/(r_{Ca-O}/2)|^2}{3e^2/r_{Ca-O}} = \frac{4}{3}\frac{e^2|S_{\sigma\sigma'}(r_{Ca-O})|^2}{r_{Ca-O}} \quad (2)$$

where $S_{\sigma\sigma'}(r_{Ca-O})$ is the overlap between the Ca-centered σ' orbital and O-centered σ orbital; note that it is a function to be evaluated at a given value of r_{Ca-O}. This crude approximation, combined with the empirically determined $H_{A\sim X}(r_c)$ matrix element of 5000 cm^{-1} at r_c = 2.16 Å, yields $|S_{\sigma\sigma'}(r = 2.16\ Å)| \approx 0.09$, which is consistent with our assumption of small overlap between Ca- and O-centered orbitals.

Determination of the Interaction Matrix Elements. From the above discussion, we see that the interaction matrix for the C*, A*, and X* states contains only two non-zero off-diagonal matrix elements: $H_{A\sim X}$ and $H_{C\sim X}$. These two matrix elements were determined by least-squares fitting, using the numerical potentials described above, at twelve points along the internuclear axis. The results are presented in Figure 2.

The variation of the two interaction matrix elements with internuclear distance can be explained qualitatively by using the Ca atomic-ion orbital parentage of the states in question, determined for the SCI model structure CaF in ref 1. The A state, from the $X\sigma\sigma'^{-1}$ configuration, is constructed from Ca^+ 4s and 4p orbitals, while the $B\sigma\sigma'^{-1}$ C state is a nearly equal mixture of Ca^+ 3d and 4p, with a small amount of 4s. The $H_{C\sim X}$ matrix element is larger than $H_{A\sim X}$ at small r_{Ca-O}, which is consistent with the C state's greater expected Ca/O overlap at small r_{Ca-O} due to the relative compactness of the 3d orbital. Similarly, $H_{A\sim X}$ becomes larger than $H_{C\sim X}$ at large r_{Ca-O} because all of the A state's electron density is in the relatively large 4s and 4p orbitals.

Extrapolation to Separated Ions: Electron Affinity of O^- and D_0^0 of CaO. In the limit of infinite r_{Ca-O}, the separated atomic-ion limit, the ground state SCI ions Ca^+ ^2S and O^- ^2P are at an energy above that of the separated neutral atoms Ca ^1S and O ^3P equal to the ionization potential of Ca minus the electron affinity of O. These two quantities have been accurately measured (6.111[13] and 1.4611 eV,[14] respectively). Likewise, the DCI separated atomic ion (Ca^{2+} ^1S and O^{2-} ^1S) asymptote should lie above the SCI asymptote by an energy equal to the ionization potential of Ca^+ minus the electron affinity of O^-. Despite the customary assignment of the most stable oxidation state of oxygen as −2, the isolated O^{2-} atomic ion is not a stable species.[15] Therefore, although the second ionization potential of Ca is a spectroscopically measured quantity (11.87 eV[13]), the second electron affinity of O is an undefined property for the free atom. The presence of O in its DCI state in a wide variety of aqueous, crystalline, and simple molecular structures suggests that we should be able to *define* the electron affinity of O^- as the energy released when an O^- ion *in the presence of a sufficiently stabilizing molecular environment* accepts an additional electron. The universal chemical importance of O^{2-} makes the measurement of an electron affinity for O^- highly desirable. For spectroscopists, knowledge of $EA(O^-)$ will enable trivial calculation of the DCI/SCI/neutral zero-order character of the low-lying states for all metal oxides.

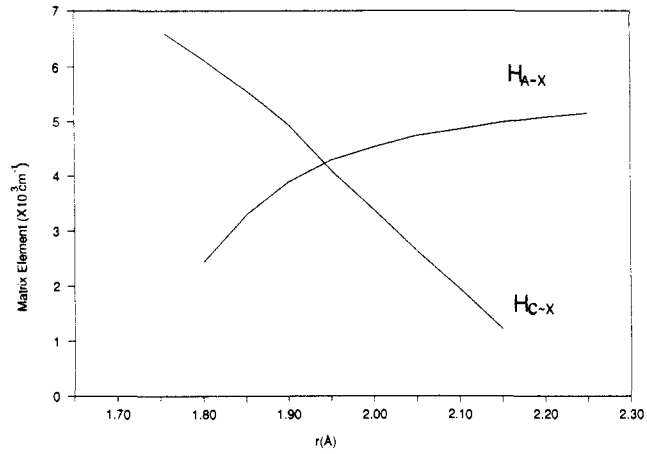

Figure 2. Interaction matrix elements $H_{A\sim X}$ and $H_{C\sim X}$ between the singly-charged ionic and doubly-charged ionic deperturbed diabatic C*, A*, and X* states of CaO calculated as functions of internuclear distance. Poorly determined values ($H_{C\sim X}$ at large r and $H_{A\sim X}$ at small r) are omitted from the plot.

Another quantity involving the relative energies of free atom pairs is the dissociation energy D_0^0 of CaO. This quantity is defined as the energy difference between the separated neutral atoms and the v = 0 vibrational level in the electronic ground state potential of the molecule. Traditional spectroscopic measurements of this quantity by extrapolation of the ground state vibrational term series (Birge–Sponer extrapolation) often fail due to neglect of avoided crossings such as the SCI∼DCI interaction discussed here.[16] The diabatic potentials derived in this work, combined with the integer-charge *atomic-ion-in-molecule* model, allow us to determine both $D_0^0(CaO)$ and $EA(O^-)$.

To derive these quantities, the diabatic potential curves must be modeled and extrapolated to infinite internuclear separation. Our *atomic-ion-in-molecule* model suggests that the deperturbed potentials can be represented by the following simple equation

$$V(R) = E(\text{atomic ions}) - \frac{Z_{Ca}Z_O e^2}{r} - \frac{e^2(\alpha_{Ca} + \alpha_O)}{2r^4} + Ae^{-(r/\rho)} \quad (3)$$

$Z_{Ca}Z_O e^2/r$ is a Coulomb attraction term, the r^{-4} term is a Rittner model derived attractive polarizability term, and $Ae^{-(r/\rho)}$ is a simplified Pauli overlap repulsion term. The Coulomb term is, in the integer-charge ionic model, exactly calculable and is by far the dominant term. The r^{-4} term requires knowledge of the free-ion polarizabilities α_{Ca} and α_O, all of which have been either

(13) Moore, C. E. *Atomic Energy Levels: As Derived From the Analyses of Optical Spectra*; Vol. I, U.S. Department of Commerce, National Bureau of Standards Circular No. 467, 1949.

(14) Neumark, D. M.; Lykke, K. R.; Andersen, T.; Lineberger, W. C. *Phys. Rev. A* **1985**, *32*, 1890–1892.

(15) Ahlrichs, R. *Chem. Phys. Lett.* **1975**, *34*, 570–574.

(16) Herzberg, G. *Molecular Spectra and Molecular Structure I*; Van Nostrand Co.: Princeton, NJ, 1953.

Table II. Fit Parameters for the X* and A* Diabatic Integer-Charge Potentials of CaO[a]

state	E_{ions}, cm^{-1}	A, cm^{-1}	ρ, Å	α_{Ca}, Å^3	α_O, Å^3
A*	72661 (100)	1.930 (3) × 10^7	0.3122 (1)	7.0 [27]	3.2 [28]
X*	204900 (120)	6.00 (5) × 10^6	0.4079 (8)	0.73 [28]	2.7 [29]

[a] Values for E_{ions}, A, and ρ are converged values (1σ uncertainties in parentheses) from least-squares fits to eq 3 in the text, where all three quantities for each potential were varied simultaneously. References [in square brackets] for polarizabilities α_{Ca} and α_O follow the values used.

measured directly or calculated. The polarizabilities used here were obtained from various sources, as summarized in Table II. The Pauli overlap repulsion terms are determined, along with the asymptotic energies, by least-squares fits to the deperturbed diabatic potentials. There are further terms in the Rittner model treatment that are not included here, due to the simplicity of our model and the wide variation of values for the needed polarizabilities in the literature. Because of the dominance of the exactly calculable Coulomb term at large r_{Ca-O}, the quantities determined with eq 3 are fairly insensitive to both the inclusion of higher terms and the exact values of the polarizabilities used.

As a result of this modeling, the energies of the neutral, SCI, and DCI ion-pairs are each located precisely with respect to the $v = 0$ level of the $X^1\Sigma^+$ ground state. The electron affinity of O^- and the dissociation energy of CaO are obtained directly from these atomic energies together with known values for EA(O), IP(Ca), and IP(Ca^+). Hence we report a value for the electron affinity of O^- of −4.53 (6) eV and a value of 35 160 (200) cm^{-1} for D_0^0 of CaO. The parameters employed in and obtained from the least-squares fits are summarized in Table II.

The electron affinity of O^- has been calculated by Herrick and Stillinger[17] to be −5.38 eV, with a resonance width of 1 eV. In their paper, they discuss the "sufficiently stabilizing molecular environment" concept and raise objections to the −7.93 eV Born–Haber cycle "measurement" of EA(O^-) by Cantor.[18] Ahlrichs[15] also describes the logical flaws in the Born–Haber cycle approach to measurement of the electron affinity of an unstable ion. Our value for EA(O^-) is in better agreement with this quantum chemical result[17] than with the previous Born–Haber cycle experimental value.[18]

The most recent measurement of the dissociation energy of CaO was made by Dagdigian,[19] who gives a lower limit of 33 300 (5600) cm^{-1}. Our reported value of 35 160 (200) cm^{-1} is in excellent agreement with this.

To obtain estimated rotation–vibration constants for the X* state the X* RKR potential was also fit with the Morse potential expression

$$V(r-r_e) = D_0(1 - e^{-\beta(r-r_e)})^2 \quad (4)$$

with use of the DCI well depth (D_0) obtained from the Rittner model fits. The value for β thus obtained was used, along with D_0 and r_e, to calculate ω_e, $\omega_e x_e$, B_e, and α_e for the X* potential according to the relations

$$\omega_e = \sqrt{2D_0\beta^2/\mu} \quad (5)$$

$$\omega_e x_e = \omega_e^2/4D_e \quad (6)$$

$$B_e = \hbar^2/2\mu r_e^2 hc \quad (7)$$

and

$$\alpha_e = \frac{6B_e^2}{\omega_e}\left[\left(\frac{\omega_e x_e}{B_e}\right)^{1/2} - 1\right] \quad (8)$$

which are all valid for a rotating Morse oscillator. These results are listed in Table I.

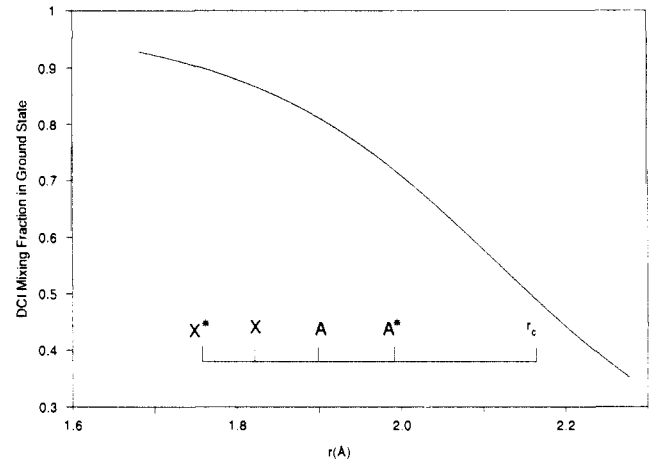

Figure 3. Mixing fraction of X* doubly-charged ionic (DCI) character in the $X^1\Sigma^+$ state of CaO. The equilibrium internuclear separations for the A, A*, X, and X* potentials and the crossing radius for the deperturbed A* and X* diabatic potentials are indicated by tick marks.

It is difficult to assign realistic uncertainties to the quantities determined here, especially EA(O^-) and D_0^0(CaO). The uncertainties cited for these quantities are 1σ values from the least-squares fits. We have made no attempt to evaluate the effects of our modeling uncertainties in the deperturbed A* and C* potential curves. The extrapolation to $v = 15$ of the A* curve, in particular, must be regarded with some suspicion. Despite these possible problems, we have been able to find readily interpretable and molecule-to-molecule transferable quantities hidden beneath the complexity of the spectrum of CaO and its plethora of multi-digit molecular constants. This has been possible due to the surprising richness and robustness of the seemingly simple integer-charge *atomic-ion-in-molecule* model.

IV. Conclusion

The extreme complexity of the electronic spectra of the diatomic metal oxides has long been a formidable obstacle for both spectroscopists and quantum chemists. Only in an extensively characterized case such as CaO have we begun to gain an understanding of global electronic structure by taking a step back from the accurately determined molecular constants and applying a simple integer-charge ionic zero-order model to the electronic properties of many experimentally analyzed electronic states. Recent ab initio calculations for similar molecules, such as MgO,[20] have taken a similar view of the interacting manifolds of diabatic states of different integer charges. Studies of the low-lying $^1\Sigma^+$ states of MgO support a picture similar to the one we have derived here for CaO from our empirical potential curves. Our fitted value for the electron affinity of O^-, in satisfactory agreement with quantum-chemical predictions,[17] should provide a stronger foundation for a model of the DCI∼SCI, SCI∼neutral, and DCI∼neutral interactions in other more complex systems such as the 3d transition-metal oxides.

Recent ab initio studies of interactions of diabatic integer-charge electronic states have included calculations of dipole moments for the adiabatic potentials near the avoided crossing.[20-23] The now well characterized DCI∼SCI interaction in CaO presents a unique opportunity to observe the dramatic change in dipole moment on going from a localized high-charge ($Ca^{2+}O^{2-}$) structure to a lower charge (Ca^+O^-) structure (in which the Ca centered valence electron is in a diffuse back-side polarized orbital) at an internuclear distance near equilibrium. In Figure 3, we display the DCI character in the $X^1\Sigma^+$ state of CaO, which changes from

(17) Herrick, D. R.; Stillinger, F. H. *J. Chem. Phys.* **1975**, *62*, 4360–4365.
(18) Cantor, S. *J. Chem. Phys.* **1973**, *59*, 5189–5194.
(19) Pedley, J. B.; Marshall, E. M. *J. Phys. Chem. Ref. Data* **1983**, *12*, 967.
(20) Thümmel, H.; Klotz, R.; Peyerimhoff, S. D. *Chem. Phys.* **1989**, *129*, 417–430.
(21) Bauschlicher, C. W., Jr.; Langhoff, S. R. *J. Chem. Phys.* **1988**, *89*, 4246–4254.
(22) Zemke, W. T.; Olson, R. E.; Verma, K. K.; Stwalley, W. C.; Liu, B. *J. Chem. Phys.* **1984**, *80*, 356–364.
(23) England, W. B. *Chem. Phys.* **1980**, *53*, 1–21.

>80% at $v = 0$ to <40% at the outer turning point of $v = 15$. These characteristics make this system uniquely suited both to calculation and verification with dc-Stark spectroscopy.[24]

We have shown that a simple atom-localized integer-charge ionic approach to diatomic molecular structures not only allows accurate prediction of state-by-state spectroscopic details[3-6] but also presents a global view of electronic structure that should be extendable from one molecule to whole families of related molecules. This deperturbation relied upon the relative simplicity and separability of our system into a single electron/single hole structure. While this simplicity may not persist for the 3d transition-metal oxides, the insight obtained from our study of intercharge interactions may provide the necessary key to interpretation and assignment of configurational parentage in these vastly more complex systems.

Acknowledgment. We thank the George R. Harrison Spectroscopy Laboratory for the use of its facilities and equipment. We are grateful to T. D. Varberg, M. C. McCarthy, and J. E. Murphy for helpful discussions. This research was supported by the National Science Foundation under Grant PHY87-09759.

(24) Rice, S. F.; Field, R. W. *J. Mol. Spectrosc.* **1986**, *119*, 331-336.
(25) Field, R. W. *J. Chem. Phys.* **1974**, *60*, 2400-2413.
(26) (a) Field, R. W.; Harris, D. O.; Tanaka, T. *J. Mol. Spectrosc.* **1975**, *57*, 107-117. (b) Dulick, M.; Bernath, P. F.; Field, R. W. *Can. J. Phys.* **1980**, *58*, 703-712.
(27) Hildenbrand, D. L. *J. Chem. Phys.* **1968**, *48*, 3657.
(28) Dalgarno, A. *Adv. Phys.* **1962**, *11*, 281.
(29) Lewis, G. V.; Catlow, C. R. A. *J. Phys. C: Solid State Phys.* **1985**, *18*, 1149-1161.
(30) Lewis, J. K.; Hougen, J. T. *J. Chem. Phys.* **1968**, *48*, 5329.
(31) Smith, F. T. *Phys. Rev.* **1969**, *179*, 111.

Enhanced Sampling in Molecular Dynamics: Use of the Time-Dependent Hartree Approximation for a Simulation of Carbon Monoxide Diffusion through Myoglobin†

R. Elber‡,§ and M. Karplus*,‡

Contribution from the Department of Chemistry, Harvard University, Cambridge, Massachusetts 02138, and Department of Chemistry, University of Illinois at Chicago, Chicago, Illinois 60680. *Received April 30, 1990*

Abstract: To obtain enhanced sampling in the study of carbon monoxide motion through myoglobin, a classical version of the time-dependent Hartree approximation is introduced. The method is derived from the Liouville equation by separating the system of interest into two parts, each of which moves in the average field of the other. In the application to myoglobin, the method makes it possible to treat a swarm of ligand molecules in the presence of a *single* trajectory for the protein. This results in a calculation that is approximately a factor of N faster than the N separate protein-ligand trajectories that would have to be used in standard simulations. Corresponding savings in time can be expected in other applications of the method to appropriate condensed phase problems. The enhanced sampling (60 CO molecules with initial positions in the heme pocket) make it possible to find widely different pathways for the escape of CO from the protein. Most of the pathways involve internal cavities that have been observed in an X-ray structure of Xe saturated myoglobin. The individual trajectories spend most of the time in the cavities; the transitions between cavities are rare events that are rapid and involve the crossing of barriers. By a comparison with the results obtained with 60 high-temperature ligands in a room-temperature protein and in a rigid protein, it is shown that even high-temperature ligands are prevented from escaping in the latter. Thus, the present results confirm the conclusion from earlier work that protein fluctuations are essential for the escape of ligands. The most important exit routes are concentrated in the region between the A, B, and E helices. Others involve the CD corner, on the proximal side of the heme and between B and G helices. A short exit path near the distal histidine found in previous simulations and supported by mutation studies is important only when the fluctuations of side chains are enhanced by increasing their temperature. This suggests that the dominant ligand pathway through the protein may depend on the system temperature.

I. Introduction

The oxygen storage and transport proteins myoglobin and hemoglobin have a binding pocket at the heme that protects the iron from the solvent in the absence of ligand.[1,2] This fact is of biological importance since water can oxidize the ferrous heme iron into the inactive ferric state.[1-3] However, as was already noted in the original X-ray structure of myoglobin,[4] the protein environment of the heme, if rigid, would prevent the entrance and the exit of ligands (e.g., oxygen, carbon monoxide) that are of approximately the same size as a water molecule. More recent high-resolution X-ray structures have confirmed that there is no obvious pathway for ligand escape in both liganded and unliganded myoglobin.[5-7] Further, empirical energy function calculations based on the crystal structures have shown that possible pathways in the neighborhood of the heme pocket have barriers on the order of 100 kcal/mol in the rigid protein;[8] such barriers would lead to escape times on the order of 10^{60} s at room temperature, infinitely long on the biological time scale. Thus, for myoglobin protein fluctuations are involved in the biological function, which requires that oxygen be able to enter and leave the heme pocket at a relatively rapid rate.

†Supported in part by a grant from the National Science Foundation (M.K.) and from the National Institutes of Health (R.E.).
‡Harvard University.
§University of Illinois at Chicago.

(1) Antonini, E.; Brunori, M. *Hemoglobin and Myoglobin and Their Reactions with Ligands*; North-Holland: Amsterdam, 1971.
(2) Bunn, H. F.; Forget, B. G. *Hemoglobin: Molecular, Genetic and Clinical Aspects*; Saunders: New York, 1980; W. B. Saunders: Philadelphia, 1986.
(3) Stryer, L. *Biochemistry*, 2nd ed.; W. H. Freeman: 1981; p 53.
(4) Perutz, M. F.; Mathews, F. S. *J. Mol. Biol. 1965, 21*, 199.
(5) Takano, T. *J. Mol. Biol.* **1977**, *110*, 537, 569.
(6) Phillips, S. E. V. *J. Mol. Biol.* **1980**, *142*, 531.
(7) Kuriyan, J.; Wilz, S.; Karplus, M.; Petsko, G. A. *J. Mol. Biol.* **1986**, *192*, 133.
(8) Case, D. A.; Karplus, M. *J. Mol. Biol.* **1979**, *132*, 343.

0002-7863/90/1512-9161$02.50/0